www.czasopisma.pan.pl PAN www.journals.pan.pl
Archives of Acoustics Vol. 47, No. 1, pp. 89–95 (2022), doi: 10.24425/aoa.2022.140735

Research Paper

Electrode Mass Loading Effects on Different Piezoelectric Substrates for Saw Delay Lines: A Comparative FEM Analysis

Sheeja P. GEORGE[(1),(2),*], Johney ISAAC[(2)], Jacob PHILIP[(3)]

[(1)] *Department of Electronics, College of Engineering*
Chengannur, Kerala, India
*Corresponding Author e-mail: sheeja@ceconline.edu

[(2)] *Department of Instrumentation, CUSAT*
Kochi, Kerala, India

[(3)] *Amaljyothi College of Engineering*
Kanjirappally, Kottayam, Kerala, India

(*received September 25, 2021; accepted December 22, 2021*)

Several modelling techniques are currently available to analyse the efficiency of inter-digital transducers (IDTs) fabricated on piezoelectric substrates for producing surface acoustic wave (SAW) devices. Impulse response method, equivalent circuit method, coupling of modes, transmission matrix method, and numerical techniques are some of the popular ones for this. Numerical techniques permit modelling to be carried out with any number of finger electrode pairs with required boundary conditions on any material of interest. In this work, we describe numerical modelling of SAW devices using ANSYS to analyse the effect of mass loading, a major secondary effect of IDTs on the performance of SAW devices. The electrode thickness of the IDT influences the resonance frequency of the SAW delay line. The analysis has been carried out for different electrode materials, aluminium, copper, and gold, for different substrate materials, barium titanate ($BaTiO_3$), X-Y lithium niobate ($LiNbO_3$), lithium tantalate ($LiTaO_3$), and the naturally available quartz. The results are presented and discussed.

Keywords: inter-digital transducers; surface acoustic wave devices; finite element analysis; numerical modelling and simulation; ANSYS.

1. Introduction

Surface acoustic wave (SAW) devices are extensively used in a variety of electronic devices such as filters, oscillators, resonators, delay lines, sensors, and actuators. The benefits of SAWs, such as low velocity and low losses, have led to the development of SAW devices in many practical systems (Campbell, 2012; Morgan, 2007). In telecommunication and wireless applications they are used as band pass filters in both IF and RF sections. As acoustic waves are highly sensitive to surface perturbations, these devices are well suited for sensor applications also. The substrate material as well as the shape of the IDT have important roles in the propagation of SAWs as there is an interaction between the electric field generated by the IDT and the mechanical strain in the substrate (Gualtieri *et al.*, 1992). The substrate material selection for SAW devices depends on the application for which it is to be implemented. A performance evaluation of IDTs for use in SAW devices has been reported in the past (Bui *et al.*, 2015). The most commonly used piezoelectric substrate materials are lithium niobate ($LiNbO_3$), lithium tantalate ($LiTaO_3$), aluminium nitride (AlN), phosphates of aluminium and gallium, and naturally available quartz.

As metallic electrodes are used as IDT, there is a reduction in the amplitude of the surface wave due to the finite mass of the metallic electrode as it modifies the surface boundary conditions (Hamidon *et al.*, 2009). The propagation of surface waves becomes altered by the mass and elastic properties of the metallic electrode and the mass loading effect is a higher order effect. The relevance of this effect is on an increase

as miniaturisation has led to greater influence of one component on neighbouring ones. So studies in these lines have great significance in the design of micrometer level SAWs.

The reduction in velocity for SAWs can be separated into three different events. The first is the velocity decrease due to mass loading and can be represented by

$$\left.\frac{\mathrm{d}v}{v}\right|_m \approx \frac{2\pi F h}{\lambda} + \frac{0.5\,K^2}{\left(1 + 0.5\,K^2 + \frac{1}{\varepsilon_r}\right)}, \tag{1}$$

where v is the acoustic velocity, h is the thickness of the metal film, λ is the acoustic wavelength, F is a constant for the substrate material employed (F = 0.037 for $LiNbO_3$ and F = 0.01 for quartz) (Schulz, Matsinger, 1972; Tancrell, 1977), and ε_r is the relative permittivity of the substrate.

Secondly, there is a decrease in velocity due to additional perturbation caused by changes in the stiffness of the surface due to deposition of the metallic IDT (Datta, 1986), and is given by

$$\left|\frac{\mathrm{d}v}{v}\right|_p = \frac{K^2}{2}. \tag{2}$$

Thirdly, the velocity shifts due to the stiffness perturbation, $\left.\frac{\mathrm{d}v}{v}\right|_s$, which depends both on the metal and the substrate used and the shift is incremental in comparison to the decrement in velocity due to mass loading.

The total velocity shift is then given by

$$\frac{\mathrm{d}v}{v} = \left.\frac{\mathrm{d}v}{v}\right|_p + \left.\frac{\mathrm{d}v}{v}\right|_m + \left.\frac{\mathrm{d}v}{v}\right|_s. \tag{3}$$

For substrates having high electro-mechanical coupling coefficient, the velocity shift is dominated by the first term of Eq. (3), as in lithium niobate. Other materials, like quartz, lithium tantalate, etc., have lower coupling coefficients, the other two terms regulate the velocity shift. The shift in velocity alters the resonance frequency by which the sensor response is evaluated (Campbell, 2012; Powell *et al.*, 2004).

The mass loading effects of IDTs have been reported earlier in literature (Yunusa *et al.*, 2014; Hamidon *et al.*, 2009; Klymyshyn *et al.*, 2009; Namdeo, Nemade, 2013; Powell *et al.*, 2004; Ramakrishnan *et al.*, 2010). Simulation techniques help to understand this second order effect and aids in the design of these devices. Simulation tools based on Finite Element Method to study the same have also been reported (Namdeo *et al.*, 2010; Zou, Lam, 2016). Coupled field analysis of commercial Finite Element Analysis tool, ANSYS, facilitates piezoelectric analysis to be carried out. The resonance frequency is observed using harmonic analysis in ANSYS. The shift in resonance frequencies of SAW delay lines with respect to the electrode thickness for selected substrate materials and selected electrode materials is presented in this paper.

2. SAW devices

SAW devices are generally operated in two configurations: resonator and delay line. In the resonator mode, a resonant cavity is formed and SAW propagates within this cavity. In the delay line configuration, two IDTs are placed separated by a distance known as delay length. One IDT acts as the transmitter and the other as receiver. The transmitter generates surface waves on excitation by electric signals, which propagate through the delay length and reaches the receiver. The receiver converts the SAW signal to electric signals and the output is tapped from it. There is a delay between the input and output signal corresponding to the separation between the IDTs. Absorbing materials are placed at the ends to eliminate unwanted reflections. The commercial production permits the operating frequency between 20 MHz and 5 GHz for such delay lines (Morgan, 2007).

2.1. Finite element simulation of SAW devices

Numerical simulations of SAW devices using finite element analysis have been reported in the literature. Finite Element Method (FEM) is a widely adopted method for 2D and 3D structures as it enables any complex geometries to be modelled for any set of material properties and applied loading, provided appropriate constitutive and equilibrium equations are fulfilled (Abraham *et al.*, 2019; El Gowini, Moussa, 2010). Lerch (1990) presented a 2D and 3D piezoelectric transducer and its response to mechanical and electrical excitations for any geometry using FEM. Atashbar *et al.* (2003) simulated the effect of mass loading with palladium sensing film for the detection of hydrogen. Ippolito *et al.* (2003) reported the analysis of acoustic wave propagation in layered SAW devices using FEM.

Commercial software like ANSYS and COMSOL are simulation tools which predict the behaviour of a system equivalent to physically realised prototypes (Ionescu, 2015). The SAW device can be configured by varying the metal pattern (IDT) on the surface of the piezo substrate as one port or two port resonators and delay lines. IDTs are patterned with a designed periodicity depending upon the frequency of operation of the device and its application. So model geometry of the device can be reduced to periodic unit cells for a 2D analysis (Abraham *et al.*, 2019; Lukose, Nemade, 2019), as shown in Fig. 1. If the entire SAW device is considered it may require large computation time and high computing facility to solve for more degrees of freedom. Further, the selection of mesh size in the FEM depends mainly on the computational resources. An increase in the number of elements per wavelength demands high computational resources and a compromise is taken in the selection. From the mesh

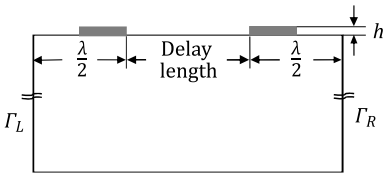

Fig. 1. Periodic geometry profile of SAW delay line used for the simulation.

optimisation study and with the available resources it is possible to have the number of mesh elements per wavelength as high as 32.

2.2. Simulation of SAW delay line

The substrate material, its crystal cut and IDT electrodes have an impact on the propagation of SAW. The substrate materials chosen are anisotropic, with the direction of crystal cut defining the properties, and are single crystal with low losses. In this simulation study barium titanate ($BaTiO_3$), X-Y lithium niobate ($LiNbO_3$), lithium tantalate ($LiTaO_3$), and naturally available quartz are chosen as substrates. The finite element analysis helps to attain an approximate model of the device through mathematical tools. Coupled field analysis in FEA is useful for solving the interaction between different physical phenomena, e.g. piezoelectrics – the interaction of electric field and structural parameters. Applying a voltage to a piezoelectric material creates a displacement, and vibrating a piezoelectric material generates a voltage. The piezoelectric equation relates the electrical and structural parameters. The coupling equation of piezoelectricity is

$$\{T\} = \left[c^E\right]\{S\} - [e]\{E\}, \tag{4}$$

$$\{D\} = [e]^{\mathrm{T}}\{S\} + \left[\varepsilon^S\right]\{E\}, \tag{5}$$

where $\{T\}$ is the stress vector, $\{S\}$ is the elastic strain vector, $\{E\}$ is the electric field intensity vector, $\{D\}$ is the electric flux density vector, $[c^E]$ is the elasticity matrix, $[e]$ is the piezoelectric stress matrix, and $[\varepsilon^S]$ is the dielectric matrix. The superscript E indicates that the constants are evaluated at a constant electric field and superscript S indicates that the constants are evaluated at a constant strain. The elasticity matrix, piezoelectric matrix, and dielectric matrix for a transversally isotropic material with polarisation in z-direction have the following forms:

$$[c] = \begin{bmatrix} c_{11} & c_{12} & c_{13} & 0 & 0 & 0 \\ & c_{22} & c_{23} & 0 & 0 & 0 \\ & & c_{33} & 0 & 0 & 0 \\ & & & c_{44} & 0 & 0 \\ & & & & c_{55} & 0 \\ & & & & & c_{66} \end{bmatrix},$$

$$[e] = \begin{bmatrix} 0 & 0 & e_{31} \\ 0 & 0 & e_{32} \\ 0 & 0 & e_{33} \\ 0 & e_{24} & 0 \\ e_{15} & 0 & 0 \\ 0 & 0 & 0 \end{bmatrix}, \qquad [\varepsilon] = \begin{bmatrix} \varepsilon_{11} & 0 & 0 \\ 0 & \varepsilon_{22} & 0 \\ 0 & 0 & \varepsilon_{33} \end{bmatrix},$$

with $c_{11} = c_{22}$, $c_{13} = c_{23}$, $c_{44} = c_{55}$, $c_{66} = \frac{(c_{11}-c_{12})}{2}$, $e_{15} = e_{24}$, $e_{31} = e_{32}$, and $\varepsilon_{11} = \varepsilon_{22}$. For quartz $e_{11} = -e_{12} = -e_{26}$, and $e_{14} = -e_{25}$.The material properties are given in Table 1. The permittivity, elasticity, and

Table 1. Substrate material properties used in the simulation.

Parameters		$BaTiO_3$ (Jaffe, Berlincourt, 1965)	X-Y $LiNbO_3$ (Warner *et al.*, 1967)	$LiTaO_3$ (Wang *et al.*, 2019)	Quartz (Bechmann *et al.*, 1962)
Elastic constants [10^{-10} N/m^2]	c_{11}	27.5	20.3	23.29	8.674
	c_{12}	17.9	5.3	4.69	0.669
	c_{13}	15.2	7.5	8.02	1.191
	c_{14}	0	0.9	−1.1	−1.1791
	c_{33}	16.5	24.5	27.53	10.72
	c_{44}	5.43	6	8.02	5.794
	c_{66}	11.3	7.5	9.3	3.988
Piezo constants	e_{15}	21.3	3.7	2.596	$e_{11} = 0.171$
	e_{31}	−2.69	0.2	0.082	$e_{14} = -0.0406$
	e_{33}	3.65	1.3	1.882	0
	e_{22}	0	2.5	1.59	0
Permittivity [C/m^2]	ε_{11}	2920	38.9	363	39.21
	ε_{33}	168	25.7	382	41.03
Density [kg/m^3]	ρ	6020	4700	4700	2649

piezoelectric constants are specified in the matrix form as indicated. The effect of electrode thickness on SAW delay line for different electrode materials is modelled. The resonance frequencies associated with SAW delay lines in each of the cases mentioned are measured and analysed to examine the effects.

2.3. Model description

The Rayleigh wave spreads along the surface of the piezoelectric substrate and decreases rapidly downwards the substrate material. Hence concentration of energy is closer to the surface. The displacement which enables wave propagation has both normal and parallel components. As Rayleigh waves are considered, the displacement in the parallel transverse direction is zero, and this enables to model the SAW devices in two dimensions (Namdeo, Nemade, 2013). The depth of the substrate can also be reduced to few wavelengths. By using appropriate periodic boundary conditions, an infinite number of IDTs can be modelled. The structural geometry used for two-dimensional simulation is shown in Fig. 1.

The coupled field analysis in ANSYS is used to simulate the SAW delay line. Here the strain in the third dimension is assumed to be zero. The dimensions used for this geometry are as follows: finger width d = 2.5 μm, wavelength λ = 10 μm, delay length L = 15 μm (1.5λ), and depth of substrate 50 μm (5λ). The thickness of the electrode is h and materials used for electrode are aluminium, copper, and gold. The material properties of the electrodes (density and permittivity) are given in Table 2. The resonance frequency is obtained with harmonic analysis and the delay time is obtained with time domain analysis (transient analysis in ANSYS). The effect on resonance frequency of the SAW delay line with respect to electrode thickness, electrode spacing, and electrode configuration are obtained for all the mentioned substrate materials and electrodes.

Table 2. Material properties of metallic electrodes (Auld, 1973).

Parameter	Aluminium	Copper	Gold
Density [kg/m^3]	2800	8960	19300
Permittivity [F/m]	9	6	6.9

2.4. Boundary conditions

For the operation of SAW delay line, the wave propagation within the device is the Rayleigh wave for which the particle displacement is in the y-direction and zero in the z-direction. So, the top surface is made stress free and the bottom is fixed. For the left and right sides of the structure periodic boundary conditions are applied and are set equal ($\Gamma_L = \Gamma_R$). For the bottom surface U_x, U_y, and V are assigned the value zero (El Gowini, Moussa, 2010; Namdeo, Nemade, 2013). Here U identifies the displacement component and V is the potential applied. The mesh size attained through the mesh convergence study is applied for all the simulations. The resonant frequency is obtained for the basic structure through harmonic analysis and the transient analysis is carried out for the verification of delay line operation at this resonant frequency.

3. Results and discussion

The harmonic analysis is carried for the basic structure to ascertain the resonant frequency. A sinusoidal signal of 10 V peak to peak is applied to the input IDT. The frequency range selected for the sinusoidal signal varies for different substrate materials. At the end of the analysis the output is taken from the output IDT. The output obtained is the amplitude of the signal in accordance with the frequency. The output amplitude will be a maximum at the resonant frequency. Theoretically the resonant frequency is given by $f_0 = \frac{c}{\lambda}$, where c is the acoustic velocity and λ is the wavelength. The resonant frequency obtained for the basic structure through harmonic analysis for the materials under consideration and the corresponding theoretical values are summarized in Table 3. The displacement profile and potential distribution at the resonant frequency in the case of lithium niobate are shown in Fig. 2.

Table 3. Comparison of theoretical and simulated values of resonant frequencies [Hz] for different substrate materials.

Materials	$BaTiO_3$	X-Y $LiNbO_3$	$LiTaO_3$	Quartz
Theoretical	550	348.8	323	315.8
Simulation	460	334.5	336	313
% variation	16.36	4.1	4.02	0.9

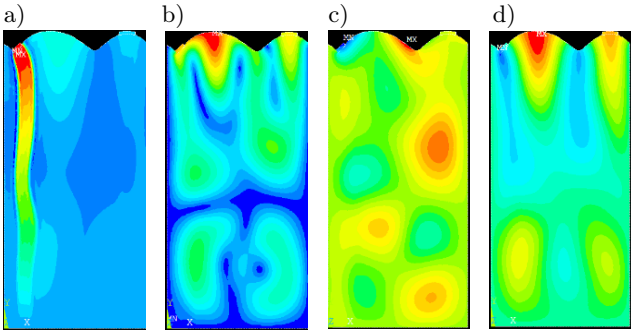

Fig. 2. a) Potential distribution, b) displacement vector sum, c) x-displacement, d) y-displacement at the resonant frequency for LN.

The SAW delay line model is verified for the delay line operation. A transient analysis is performed for this purpose, and a sinusoidal signal of amplitude 10 V is applied to the input IDT for 200 ns. The output obtained from the receiver IDT discloses the delay between the input and output voltages. Theoretically,

the delay time between the input and output IDTs is given by $\tau = \frac{L}{v}$, where L is the delay length and v is the acoustic velocity. Table 4 shows the theoretical and simulated values of delay times for the SAW structures based on the chosen materials. The closeness of the theoretical and simulated values establishes the validity of ANSYS in the piezoelectric analysis.

Table 4. Comparison of theoretical and simulated values of delay times for different substrate materials [ns].

Materials	$BaTiO_3$	X-Y $LiNbO_3$	$LiTaO_3$	Quartz
Theoretical	2.7	3.75	4.64	4.75
Simulation	2.5	3.31	4.35	4.38
% variation	7.4	11.73	6.25	7.78

3.1. Effect of electrode thickness

In SAW devices the metallic electrodes fabricated onto the surface strongly affect the propagation of acoustic waves (Gamble, Malocha, 2002). Acoustic waves gets perturbed when it passes beneath the metallic IDT. The metallic IDT imparts a mechanical loading or mass loading effect. Mass loading effect has been reported in literature by many researchers (Gamble, Malocha, 2002; Hamidon *et al.*, 2009). Auld's perturbation theory explains the mass loading (Morgan, 2007) effect. This section describes the simulation that was performed to study the mass loading effect of the electrodes by varying the thickness of the electrodes, as outlined below.

Single IDT configuration with λ = 10 µm is considered for this analysis. In order to study the effect of electrode thickness, the thickness is varied from 0.1 µm to 2 µm, which makes the normalized thickness of the electrode (h/λ) from 0.01 to 0.2. For each of the substrate material, $BaTiO_3$, X-Y $LiNbO_3$, $LiTaO_3$, and quartz, three metal electrode types, Al, Cu, and Au, have been considered. The plots of resonance frequency and normalised thickness in each of these cases are shown in Fig. 3.

From Fig. 3, it can be observed that the shift in resonant frequency is lower for aluminium while it is higher for gold, irrespective of the substrate type. The resonance frequency shifts for normalised electrode thickness of 0.01 to 0.2 µm for different substrate materials are different and are detailed in Table 5. It can be seen that for the electrode thickness up to 0.05 µm ($h/\lambda = 0.5$) this value is negligible and becomes significant after this. When the electrode thickness becomes larger the loading effect on resonant frequency is fully dependent on the density of the metal. Heavier metals impart a stronger loading effect on transduction mechanism, and affect the resonant frequency.

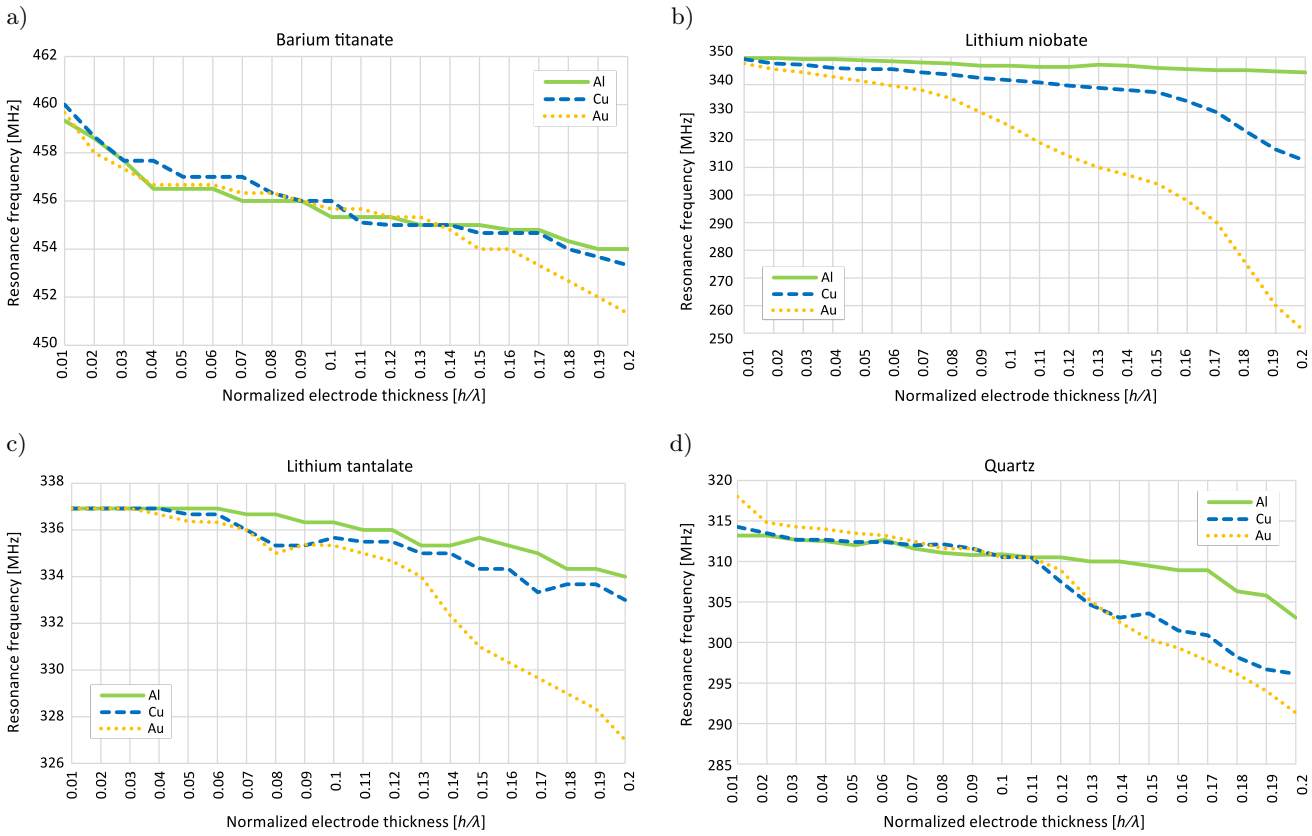

Fig. 3. Resonance frequency for normalised electrode thickness for different substrate materials: a) $BaTiO_3$, b) X-Y $LiNbO_3$, c) $LiTaO_3$, d) quartz.

Table 5. Shift in resonance frequency for normalised electrode thickness of 0.01 to 0.2 μm for different substrate materials with respect to electrode type.

Piezoelectric substrate	Shift in resonance frequency with respect to electrode type [MHz]		
	Al	Cu	Au
$BaTiO_3$	5.33	6.67	7.34
X-Y $LiNbO_3$	5.2	36.8	97.2
$LiTaO_3$	2.92	3.92	9.92
Quartz	10.13	18.14	26.67

Considering the normalised electrode thickness of 0.01 and 0.2 μm, there is a shift in resonance frequency among different substrate materials, and is detailed in Table 6. Here the effect of both metallic electrode and the substrate material is significant. Hence the third term of Eq. (3), which is influenced by both metal and substrate properties, becomes prominent. The velocity shift depends on density and stiffness of the material and its value becomes invalid for a strong piezoelectric material like $LiTaO_3$ (Powell *et al.*, 2002).

Table 6. Shift in resonance frequency for different substrate materials with respect to normalised electrode thickness.

Piezoelectric substrate	Shift in resonance frequency [MHz] with respect to normalized electrode thickness
$BaTiO_3$	2.04
X-Y $LiNbO_3$	92
$LiTaO_3$	7
Quartz	6.74

According to Eq. (3) the first and second term depends on the electromechanical coupling coefficient and hence the high K^2 $LiNbO_3$ with high density gold electrodes is more sensitive to the mass loading. Because of this, light aluminium electrodes are preferred for the commercial use rather than heavier metals. From the displacement profile obtained it is evident that the displacement in the perpendicular direction is bigger than that in the horizontal direction.

4. Conclusion

Simulations are performed using the FEA tool ANSYS to analyse the effect of electrode thickness on SAW delay line configurations. The analysis shows that there is a strong dependency for resonant frequency on the electrode thickness. Analysis is carried out for three different metal electrodes, Al, Cu, and Au, and for substrate materials of $BaTiO_3$, X-Y $LiNbO_3$, $LiTaO_3$, and quartz. The loading effect of the electrodes becomes significant when thickness increases for heavier metals. Hence density of the electrode need be considered as it has an effect on the resonant frequency. The results of this study give an insight into the design consideration and choice of electrodes for the design of SAW delay lines. Mass loading becomes a convenient means for frequency adjustments during the design phase.

References

1. Abraham N., Krishnakumar R., Unni C., Philip D. (2019), Simulation studies on the responses of ZnO-CuO/CNT nanocomposite based SAW sensor to various volatile organic chemicals, *Journal of Science: Advanced Materials and Devices*, **4**(1): 125–131, doi: 10.1016/j.jsamd.2018.12.006.
2. Atashbar M.Z., Bazuin B.J., Krishnamurthy S. (2003), Design and simulation of SAW sensors for wireless sensing, *Proceedings of IEEE Sensors 2003*, **1**(1): 584–589, doi: 10.1109/ICSENS.2003.1279005.
3. Auld B.A. (1973), *Acoustic Fields and Waves in Solids*, John Wiley & Sons: New York.
4. Bechmann R., Ballato A.D., Lukaszek T.J. (1962), Higher-order temperature coefficients of the elastic stiffinesses and compliances of alpha-quartz, *Proceedings of the IRE*, **50**(8): 1812–1822, doi: 10.1109/JRPROC.1962.288222.
5. Bui T.H., Duc T.B., Duc T.C. (2015), An optimisation of IDTs for surface acoustic wave sensor, *International Journal of Nanotechnology*, **12**(5/6/7): 485–495, doi: 10.1504/IJNT.2015.067906
6. Campbell C. (2012), *Surface Acoustic Wave Devices and Their Signal Processing Applications*, Academic Press: San Diego.
7. Datta S. (1986), *Surface Acoustic Wave Devices*, Prentice-Hall: Englewood Cliffs.
8. El Gowini M.M., Moussa W.A. (2010), A finite element model of a MEMS-based surface acoustic wave hydrogen sensor, *Sensors*, **10**(2): 1232–1250, doi: 10.3390/s100201232.
9. Gamble K.J., Malocha D.C. (2002), Simulation of short LSAW transducers including electrode mass loading and finite finger resistance, *IEEE Transactions on Ultrasonics, Ferroelectrics, and Frequency Control*, **49**(1): 47–56, doi: 10.1109/58.981383.
10. Gualtieri J.G., Kosinski J.A., Ballato A. (1992), Piezoelectric materials for saw applications, *IEEE 1992 Ultrasonics Symposium Proceedings*, pp. 403–412, Arizona, doi: 10.1109/ultsym.1992.275972.
11. Hamidon M.N., Mousavi S.A., Isa M.M., Ismail A., Mahdi M.A. (2009), Finite element method on mass loading effect for gallium phosphate surface acoustic wave resonators, *Proceedings of the World Congress Engineering*, **1**: 447–452, London.
12. Ionescu V. (2015), Design and analysis of a Rayleigh saw resonator for gas detecting applications, *Romanian Journal of Physics*, **60**(3–4): 502–511.

13. Ippolito S.J., Kalantar-Zadeh K., Powell D.A., Wlodarski W. (2003), A 3-dimensional approach for simulating acoustic wave propagation in layered SAW devices, *IEEE Symposium on Ultrasonics*, **1**: 303–306, Honolulu, HI, USA, doi: 10.1109/ULTSYM.2003.1293411.

14. Jaffe H., Berlincourt D.A. (1965), Piezoelectric transducer materials, *Proceedings of the IEEE*, **53**(10): 1372–1386, doi: 10.1109/PROC.1965.4253.

15. Klymyshyn D.M., Kannan T., Kachayev A. (2009), Finite element modelling of electrode mass loading effects in longitudinal leaky SAW resonators, *Microwave and Optical Technology Letters*, **51**(21): 390–395, doi: 10.1002/mop.24042.

16. Lerch R. (1990), Simulation of piezoelectric devices by two-and three-dimensional finite elements, *IEEE Transactions on Ultrasonics, Ferroelectrics, and Frequency Control*, **37**(3): 233–247, doi: 10.1109/58.55314.

17. Lukose V., Nemade H.B. (2019), Finite element simulation of one-port surface acoustic wave resonator with thick interdigital transducer for gas sensing, *Microsystem Technologies*, **25**(2): 441–446, doi: 10.1007/s00542-018-4015-y.

18. Morgan D. (2007), *Surface Acoustic Wave Filters with Applications to Electronic Communications and Signal Processing*, Academic Press.

19. Namdeo A.K., Nemade H.B. (2013), Simulation on effects of electrical loading due to interdigital transducers in surface acoustic wave resonator, *Procedia Engineering*, **64**: 322–330, doi: 10.1016/j.proeng.2013.09.104.

20. Namdeo A.K., Nemade H.B., Ramakrishnan N. (2010), FEM simulation of generation of bulk acoustic waves and their effects in saw devices, *Proceedings of the COMSOL Conference*, Bagalore, India.

21. Powell D.A., Kalantar-Zadeh K., Ippolito S.J., Wlodarski W. (2002), A layered SAW device based on ZnO/LiTaO/sub 3/ for liquid media sensing applications, *IEEE Ultrasonics Symposium*, **1**: 493–496, Munich, Germany, doi: 10.1109/ULTSYM.2002.1193449.

22. Powell D.A., Kalantar-Zadeh K., Wlodarski W. (2004), Numerical calculation of SAW sensitivity: application to ZnO/LiTaO3 transducers, *Sensors and Actuators A: Physical*, **115**(2–3): 456–461, doi: 10.1016/j.sna.2004.05.031.

23. Ramakrishnan N., Palathinkal R. P., Nemade H.B. (2010), Mass loading effects of high aspect ratio structures grown over saw resonator, *Sensor Letters*, **8**(2): 253–257, doi: 10.1166/sl.2010.1258.

24. Schulz M.B., Matsinger J.H. (1972), Rayleigh-wave electromechanical coupling constant, *Applied Physics Letters*, **20**: 367–369, doi: 10.1063/1.1654190.

25. Tancrell R.H. (1977), Principles of surface wave filter design, [in:] *Surface Wave Filters: Design Construction and Use*, Mathews H. [Ed.], pp. 109–164, Wiley Interscience, New York.

26. Wang T., Green R., Guldiken R., Wang J., Mohapatra S., Mohapatra S.S. (2019), Finite element analysis for surface acoustic wave device characteristic properties and sensitivity, *Sensors*, **19**(8): 1749, doi: 10.3390/s19081749.

27. Warner A.W., Onoe M., Coquin G.A. (1967), Determination of elastic and piezoelectric constants for crystals in class (3 m), *The Journal of the Acoustical Society of America*, **42**: 1223–1231, doi: 10.1121/1.1910709.

28. Yunusa Z., Hamidon M.N., Kaiser A., Awang Z. (2014), Gas sensors: A review, *Sensors and Transducers*, **168**(4): 61–75, doi: 10.13074/jent.2015.12.153163.

29. Zou J., Lam C.S. (2016), Electrode design of AlN lamb wave resonators, *IEEE International Frequency Control Symposium (IFCS)*, pp. 1–5, New Orleans, USA, doi: 10.1109/FCS.2016.7563573.